

## **17. TITAN-II DIVERTOR ENGINEERING**

Patrick I. H. Cooke  
Richard L. Creedon

Charles C. Bathke  
Steven P. Grotz  
Shahram Sharafat

James P. Blanchard  
Mohammad Z. Hasan

## Contents

17.1.	INTRODUCTION . . . . .	17-1
17.2.	MATERIALS . . . . .	17-4
17.2.1.	Plasma-Facing Material . . . . .	17-4
17.2.2.	Divertor-Target Coolant . . . . .	17-5
17.2.3.	Substrate Material . . . . .	17-5
17.3.	TARGET FABRICATION . . . . .	17-6
17.3.1.	Reference Design . . . . .	17-6
17.3.2.	Alternative Design . . . . .	17-8
17.3.3.	Discussion . . . . .	17-10
17.4.	TARGET DESIGN . . . . .	17-10
17.5.	THERMAL AND STRUCTURAL ANALYSES . . . . .	17-17
17.5.1.	Thermal Analysis . . . . .	17-19
17.5.2.	Stress Analysis . . . . .	17-22
17.6.	DIVERTOR-COIL ENGINEERING . . . . .	17-25
17.7.	VACUUM SYSTEMS . . . . .	17-27
17.8.	SUMMARY AND CONCLUSIONS . . . . .	17-27
	REFERENCES . . . . .	17-29

## 17. TITAN-II DIVERTOR ENGINEERING

### 17.1. INTRODUCTION

This section describes the engineering design of the divertor of TITAN-II, including the thermal and mechanical design of the divertor components, materials selection, and fabrication issues. The design of the impurity-control system poses some of the most severe problems of any component of a DT fusion reactor. For TITAN, the divertor design represents (perhaps together with the design of the oscillating-field current-drive system, described in Section 7) the most critical engineering and physics issues for the reactor.

The two main design issues for the divertor system are to achieve heat loadings on the divertor collector plate (or target) that do not exceed the maximum acceptable level, while simultaneously ensuring that the sputtering erosion rate does not lead to an early failure of the component. These two aims tend to conflict, because the high heat loadings which inevitably occur on the divertor target require the use of thin structures to minimize temperature differences and thermal stresses, while a thick structure is necessary to give a long life against erosion.

The background behind the toroidal-field-divertor design for TITAN-I was given in Section 11; the considerations for TITAN-II are the essentially the same. An account of the magnetic analysis for the divertor is contained in Section 4.4 and the edge-plasma and neutral-particle modeling, which had a strong bearing on the engineering of the divertor, are described in Sections 5.4 and 5.5, respectively.

As discussed in Section 4.4, the TITAN divertor uses an “open” configuration in which the divertor target is located close to the null point, facing the plasma, rather than in a separate chamber. This positioning takes advantage of the increased separation between the magnetic field lines (flux expansion) in this region, which tends to reduce the heat loading on the divertor plate because the plasma flowing to the target is “tied” to the field lines. The high plasma density in front of the divertor target ensures that the neutral particles emitted from the surface have a short mean free path; a negligible fraction of these neutral particles enter the core plasma (Section 5.5).

The magnetic design (Section 4.4) focussed on maximizing the achievable degree of flux expansion in order to minimize the peak heat flux on the divertor target while

minimizing the divertor-coil currents and reducing the joule losses in the divertor coils. The toroidal-field-coil design for TITAN-II, which consists of copper coils as opposed to the integrated blanket coils (IBCs) of TITAN-I, prompted a new divertor magnetic design. The final magnetic design, similar to that of TITAN-I, includes three divertor modules, located  $120^\circ$  apart in the toroidal direction. An equatorial-plane cross section of a quadrant of the TITAN-II fusion power core including one of the divertors is shown in Figure 17.1-1. The magnetic field lines are diverted onto the divertor plate using one nulling and two flanking coils which localize the nulling effect. No divertor-trim coils are required for the TITAN-II design. The use of copper coils reduces the joule losses in the TITAN-II divertor coils to 9.8 MW which are much smaller than that of the TITAN-I IBC divertor coils (120 MW).

The results of the magnetic design of TITAN-II divertor (*e.g.*, field-line connection length) were not sufficiently different from the results for TITAN-I to warrant a separate edge-plasma analysis. A summary of the results of the edge-plasma modeling for TITAN-I, which are also used for the TITAN-II design, is given in Table 17.1-I and are described in detail in Section 5.4. The plasma power balance is controlled by the injection of a trace amount of a high atomic-number impurity (xenon) into the plasma, causing strong radiation from the core plasma, the scrape-off layer (SOL) plasma, and the divertor plasma. About 95% of the steady-state heating power (alpha particle and ohmic heating) can be radiated to the first wall and divertor plate, with about 70% being radiated from the core plasma (*i.e.*, inside the separatrix). This intense radiation reduces the power deposited on the divertor target by the plasma to an acceptably low level. Preliminary experimental results suggest that beta-limited RFP plasmas can withstand a high fraction of power radiated without seriously affecting the operating point (Section 5.3); this behavior contrasts with that observed in tokamaks, in which a high radiation fraction appears to lead to a plasma disruption. The radiative cooling also reduces the electron temperature at the first wall and divertor target (also assisted by recycling) which, in turn, reduces the sputtering erosion problem.

The final TITAN-II divertor design represents the results of extensive iterations between edge-plasma analysis, magnetic design, thermal-hydraulic and structural analyses, and neutronics. The remainder of this section is devoted to the engineering aspects of this integrated design. In many cases, there are strong similarities with the TITAN-I design. The major difference between TITAN-I and TITAN-II divertor designs is the use of an aqueous-salt solution as the coolant for the TITAN-II divertor (as opposed to liquid lithium for TITAN-I). The use of a nonconducting coolant eliminates the concerns of excessive MHD pressure drops. As a result, the divertor target can be shaped more freely,

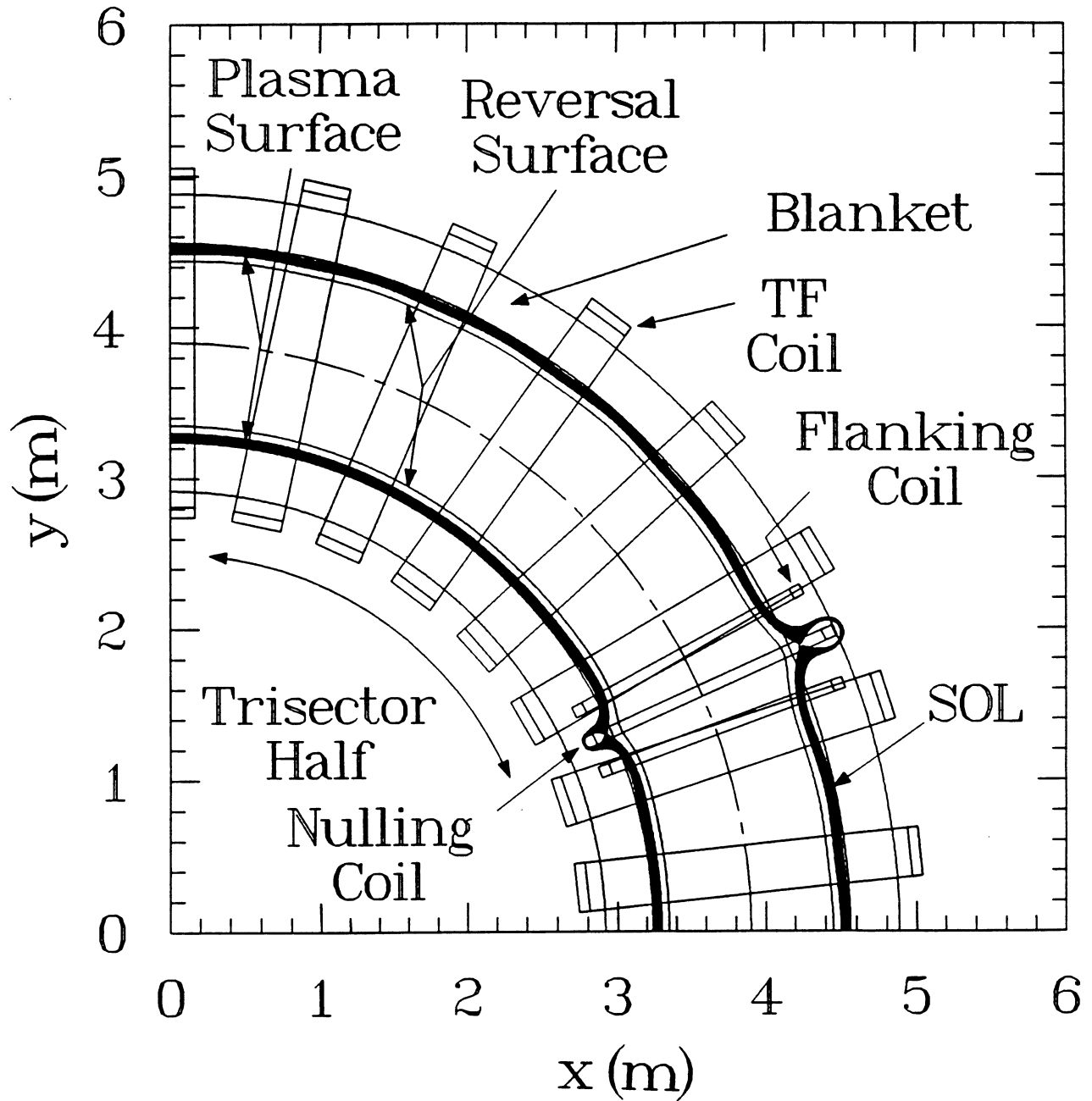


Figure 17.1-1. Equatorial-plane view of divertor coils and magnetic field lines for TITAN-II.

Table 17.1-I.

## SUMMARY OF TITAN-II EDGE-PLASMA CONDITIONS

---

Number of divertors	3
Scrape-off layer thickness	6 cm
Peak edge density	$1.7 \times 10^{20} \text{ m}^{-3}$
Peak edge ion temperature	380 eV
Peak edge electron temperature	220 eV
Plasma temperature at first wall	1.7 eV
Peak divertor density	$6 \times 10^{21} \text{ m}^{-3}$
Peak divertor plasma temperature	4.5 eV
Divertor recycling coefficient	0.995

---

resulting in a rather lower peak heat flux for the TITAN-II divertor. Furthermore, the coolant for the TITAN-II divertor can be routed in the radial/toroidal direction, making the divertor performance less sensitive to the exact location of the plasma. Lastly, a single structural material (tungsten alloy) can be used both for the divertor armor and the divertor-coolant channels, easing the divertor-target design and fabrication.

## 17.2. MATERIALS

### 17.2.1. Plasma-Facing Material

In order to reduce the erosion of the divertor armor by the plasma, a high atomic-number ( $Z$ ) material must be used for the surface of the divertor plate. This conclusion is based on the estimates of sputtering rates of various candidate materials (described in Section 5.5). The threshold energy for sputtering is sufficiently high for high- $Z$  materials that the erosion rate of the divertor target under the expected conditions for TITAN designs (Table 17.1-I) is acceptable.

The requirements for the plasma-facing material are identical to those described for TITAN-I in Section 11.2. Thus, the same alloy of tungsten and rhenium, W-26Re, as was used for TITAN-I, has been chosen for the TITAN-II divertor armor. The properties of this alloy are described in Section 11.2 and are summarized in Table 11.2.-I.

### 17.2.2. Divertor-Target Coolant

It is advantageous to use the same coolant for all components of the fusion power core (FPC). Therefore, an aqueous-LiNO<sub>3</sub> solution (as used in the blanket) is chosen as the divertor-target coolant for TITAN-II. Pure water was also considered because of the eased corrosion and radiolysis problems, but these concerns appear to have been accounted for in the blanket-coolant analysis (Section 16.2). Also, there is a large uncertainty in the thermal and physical properties of the salt solution (Section 16.2), but the indications are that the changes relative to pure water should improve the thermal performance (*e.g.*, by allowing operation at a lower pressure and increasing the critical heat flux). The choice of an LiNO<sub>3</sub> solution as the TITAN-II divertor-target coolant, therefore, allows an assessment of the potential of aqueous-salt solutions, but it is recognized that certain issues cannot be fully resolved until more experimental data are available. The concentration of the coolant is the same as for the blanket (6.4 at.% Li), but because of the higher loadings on the divertor, different inlet and outlet conditions have to be used. In particular, as described in Section 17.4, the higher pressure used for the divertor coolant allows a higher outlet temperature. This permits the heat deposited into the divertor-target coolant to be extracted via a heat exchanger with the blanket inlet coolant, and avoids the need for a complete separate cooling circuit.

### 17.2.3. Substrate Material

Using a single structural material for the divertor target avoids the problems of bonding dissimilar materials and stress concentrations which can occur at the interface of the two materials (Section 11.5). Such a construction was not possible for TITAN-I because of MHD pressure-drop considerations, but has been chosen for TITAN-II in order to compare the two approaches. Therefore, the coolant tubes for the divertor target are also made from the W-26Re alloy which was selected for the divertor armor. The complex geometry of the target plate does not allow the structure to be fabricated from one piece, so the sputtering-resistant armor plate is bonded to the coolant tubes, as described in Section 17.3.

### 17.3. TARGET FABRICATION

In the TITAN-II divertor, the divertor-target coolant is routed in the radial/toroidal direction, in order to make divertor performance less sensitive to the exact location of the plasma (Section 17.4). A schematic view of the TITAN-II divertor geometry is presented in Figure 17.3-1 and shows the coolant-flow paths and headers. Because of the double curvature of the divertor plate, the cross section of the coolant tubes must vary along their length in order for the tubes to continue to touch. To avoid severe difficulties in the fabrication of the tungsten-rhenium tubes with variable cross sections, the reference design for the TITAN-II divertor plate uses constant-cross-section tubes, with coolant tubes arranged to touch only at the apex of the target (the location of minimum minor radius), with a slight gap between adjacent tubes at other points (Figure 17.3-1). This choice is made because the thermal penalties associated with this approach appear manageable (Section 17.5).

Various procedures which were considered for the fabrication of the divertor plate are discussed in Section 17.3.1. As an alternate design, methods of manufacturing tubes of variable cross section have been examined, and are described in Section 17.3.2.

#### 17.3.1. Reference Design

The reference fabrication procedure for the TITAN-II divertor plate follows fairly closely that of TITAN-I (Section 11.4). The first step involves the production of a 3- to 4-mm-thick W-26Re plate using powder-metallurgy techniques. After allowances have been made for thermal-expansion effects between the bending temperature and the operational temperature, the plate is bent to accord with the specified target shape. Grooves for the coolant channels are then formed in the plate using a numerically controlled milling procedure. This leaves a minimum plate thickness of 1 mm at the apex of the coolant tube, with a greater thickness between tubes. The W-26Re coolant tubes (which are themselves manufactured using powder-metallurgy techniques) are then brazed into the grooves, using a CuPd18 braze alloy [1] with an application temperature of  $\sim 1100^\circ\text{C}$ . The ends of the W-26Re tubes are interconnected by brazing them to poloidal headers at the inlet and outlet (Figure 17.3-1).

Another approach to the fabrication of the armor is to use chemical-vapor deposition (CVD) to deposit the armor onto the bank of coolant tubes. At conventional deposition rates of between 1 to 3 mm/h, this process would not take a long time. After completion of the deposition, the resulting uneven surface is ground to yield the necessary flat,

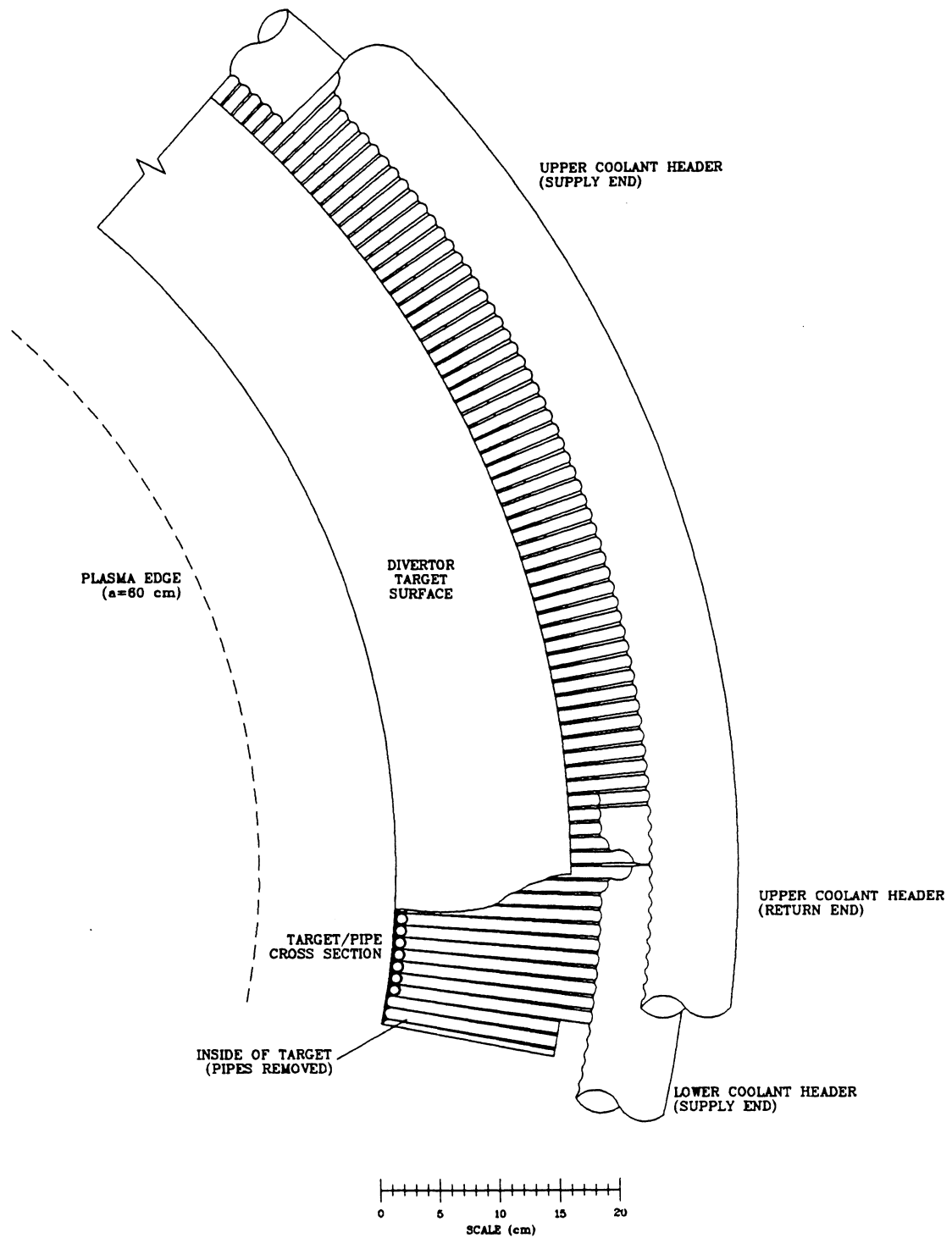


**Figure 17.3-1.** Schematic view of the divertor geometry, showing the divertor target, coolant-flow paths, and headers.

smooth surface. Silicon carbide wheels with grain sizes of 100 to 120  $\mu\text{m}$  have proven useful for most grinding applications [2].

### 17.3.2. Alternative Design

This subsection describes methods of manufacturing the divertor plate with variable-cross-section coolant tubes to eliminate the gaps between the coolant tubes. Two manufacturing processes have been identified to make such tubes: hydroforming and CVD. After individual tubes are manufactured, they are brazed together using the CuPd18 braze alloy (Section 17.3.1) and then joined to the poloidal ring headers. The free-standing structure of W-26Re tubes with headers constitutes the skeleton of the divertor plate. The divertor armor is then attached to the bank of tubes using the CVD method or by brazing (as discussed in Section 17.3.1).

#### 17.3.2.1. Hydroforming

The high ductility of tungsten-rhenium alloys (Table 11.2-I) allows the fabrication of pre-bent tubes with variable cross sections by hydroforming. Hydroforming is particularly useful when tubes of variable cross section also need to be bent because it avoids the problem of distortion of the cross section which frequently arises with bending.

As an example, the space shuttle main engine (SSME) is made of a number of variable-diameter hexagonal tubes that resemble giant bows ( $\sim 3\text{-m}$  high) for cooling purposes. These tubes are manufactured using the hydroforming technique. First, a mold is made of the final product in two halves. For the SSME, these molds have semi-hexagonal grooves in the shape of the bow. A circular tube (Inconel) is bent to fit more or less into the groove. The mold halves are closed and the tube is pressurized. Plastic deformation of the tube would produce the variable cross section and the overall bend with very close tolerances. The nonuniform hexagonal bowed tubes are then welded together to form a channel-walled Venturi tube for the SSME [3].

Hydroforming of tungsten-rhenium alloys at temperatures above  $1000^\circ\text{C}$  is particularly attractive because of the high ductility of these alloys ( $\sim 70\%$  at  $1500^\circ\text{C}$ ). The great advantage of using hydroforming is that the variable-cross-section tubes eliminate the gaps between the tubes that may be caused by sharp bends.

### 17.3.2.2. Chemical-vapor deposition of tungsten

Chemical-vapor deposition (CVD) is another process which can be used to manufacture variable-cross-section tungsten-rhenium tubes. The CVD technique (Section 11.4) involves the deposition of target material onto a hot substrate (400 to 1000 °C). The CVD of tungsten has been investigated more thoroughly than CVD of any other metal, and is widely used in various industries for many important applications [4]. The most frequently used CVD process is the hydrogen reduction of the halides  $WF_6$  and  $WCl_6$ . An example of the overall hydrogen reduction of hexafluoride to tungsten is:



The versatility of the CVD process and the control over the end-product characteristics is reflected in the number of papers that have been published on chemical-reaction parameters, kinetics, thermodynamics, pressure and temperature factors, substrate effects, deposit orientation, and industrial applications. In particular, numerous articles on the CVD of tungsten and tungsten-rhenium alloys appear in the literature [5-9]. Free-standing structural components are routinely manufactured using CVD of tungsten and tungsten-rhenium for high-temperature applications [10-20]. The tungsten alloy is chemical-vapor deposited onto a mandrel which is later removed, either by chemical etching or by melting. Mandrels of variable-cross-section coolant tubes would have to be manufactured for each tube individually.

The mechanical properties of tungsten-rhenium tubes produced by the CVD process have been studied and compared with those produced by the powder-metallurgy technique since the late 1960s [13-19]. Early samples of CVD tungsten showed a high degree of columnar grains and voids in the direction of deposition. It was shown that the low-temperature mechanical properties of the early CVD tungsten samples were comparable to those of tungsten produced by powder metallurgy [14]. However, creep-rupture tests at 1650 and 2200 °C clearly showed differences between the mechanical properties of the early CVD samples and powder-metallurgy tungsten [13].

An extensive study of tungsten-rhenium deposition was later conducted by Holman and Huegel [15-17]. Their studies greatly elucidated the effects of temperature, pressure, gas mixture, and total gas-flow rates on the composition, deposition rate, and grain structure of the deposited tungsten-rhenium alloys. They developed a CVD technique that produced fine-grained tungsten-rhenium alloys with no preferential grain-growth direction and with densities of 98.5% to 99% of the theoretical density. These figures are higher than those obtained in samples produced by powder metallurgy or plasma

spraying [19]. The new deposition techniques include simple rubbing or brushing of the deposit surface during deposition with a tungsten-carbide rod or a tungsten-wire brush. Thirty-centimeter-long tubes of tungsten-rhenium alloys with various rhenium contents (up to 28% rhenium) were chemical-vapor deposited onto mandrels with an outer diameter of 1 cm, with deposition rates of up to 1 mil/m (1.5 mm/h). Using Holman and Huegel techniques, CVD tubing can be produced with mechanical properties equal to those obtained in wrought or powder-metallurgy tungsten-rhenium alloys.

### 17.3.3. Discussion

Several fabrication methods have been identified for the TITAN-II divertor plates, and the reference-fabrication procedure is based on brazing a bank of constant-cross-section coolant tubes into the grooves milled on a powder-metallurgy-produced tungsten-rhenium plate. A particularly promising alternative method is the hydroforming process, which allows "bowed" tungsten-rhenium tubes with variable cross sections to be produced, followed by CVD of tungsten-rhenium armor to form the target plate. Although the individual processes involved in the manufacturing of the divertor plates are feasible and are used commercially, the viability of the total manufacturing process needs to be researched and be demonstrated. In particular, CVD furnaces large enough to hold the TITAN-II divertor plate need to be developed.

## 17.4. TARGET DESIGN

The details of the shaping of the surface and the overall thermal analysis are described in this section; a more extensive set of structural and thermal analyses using finite-element techniques is reported in Section 17.5.

Despite the intense radiation arising from the impurities injected into the plasma, careful shaping of the divertor target is required to maintain the heat flux at acceptable levels at all points on the plate. The target design for TITAN-II proceeds in much the same way as for TITAN-I (Section 11.4). This complex problem is handled by a modified version of the code described in Section 11.4. The differences arise from the use of an aqueous-salt solution as the coolant (eliminating the MHD effects), and using the tungsten-rhenium alloy as the structural material for the divertor-plate coolant tubes which allows for much higher temperatures in the tube walls.

The geometry of the TITAN-II divertor, representing the results of the iteration between the thermal analysis and the shaping code, is shown in Figure 17.4-1. This

geometry is very similar to that of TITAN-I with the following differences: (1) copper coils are used here rather than divertor IBCs; (2) the shape of the target is somewhat different because the use of a nonconducting coolant removes the MHD constraints on locating the target in regions of minimum magnetic field. Figure 17.4-2 shows the inclination angle of the target to the magnetic field lines and the flux-expansion factor as a function of distance along the target (measured from the apex of the target). A comparison with the corresponding figures for TITAN-I shows that the trends are similar. However, because the MHD constraints are removed, slightly lower inclination angles are possible for TITAN-II, allowing the area of the target to increase and a rather lower peak heat flux to be obtained.

For TITAN-II, the divertor-target coolant flows in the radial/toroidal direction, as opposed to the poloidal direction which was mandated for TITAN-I in order to avoid excessive MHD pressure drops. A disadvantage of the poloidal coolant routing (or, in general, the direction along the majority magnetic field) is that the heating rate can vary considerably from one tube to another. If the plasma should move slightly from its expected position, a coolant tube could receive a much greater heat load than it was designed for. With the coolant flowing in the direction perpendicular to the majority field, the total heat deposited on each tube is the same, and plasma motion will only alter the heat-flux distribution along the length of the tube. A problem with the toroidal/radial flow proposed for TITAN-II is that the length of the tubes is rather short, which can lead to a large volumetric flow rate of the coolant and a small inlet-to-outlet temperature rise. This problem, however, is avoided in TITAN-II design by using poloidal ring headers and a multi-pass coolant flow, as illustrated in Figure 17.3-1.

Because of the double curvature of the divertor plate, the cross section of the coolant tubes must vary along their lengths in order for the tubes to remain touching. Because of severe difficulties in the fabrication of the variable-cross-section tungsten-rhenium tubes, the reference divertor-plate design of TITAN-II uses constant-cross-section tubes, arranged to touch only at the apex of the target (the location of minimum minor radius), with a slight gap between adjacent tubes at other points (Figure 17.3-1). The effects of these gaps on the thermal and stress analyses are discussed in detail in Section 17.5, but the results of these more sophisticated analyses were incorporated into the overall design which is described here.

The diameter of each coolant tube was chosen to be as large as possible (to minimize the number of tubes and, hence, the likelihood of failure at the ends of the tubes where they are joined to the steel headers), taking into account pressure and thermal stress considerations. This process led to a coolant-tube design with an outer diameter

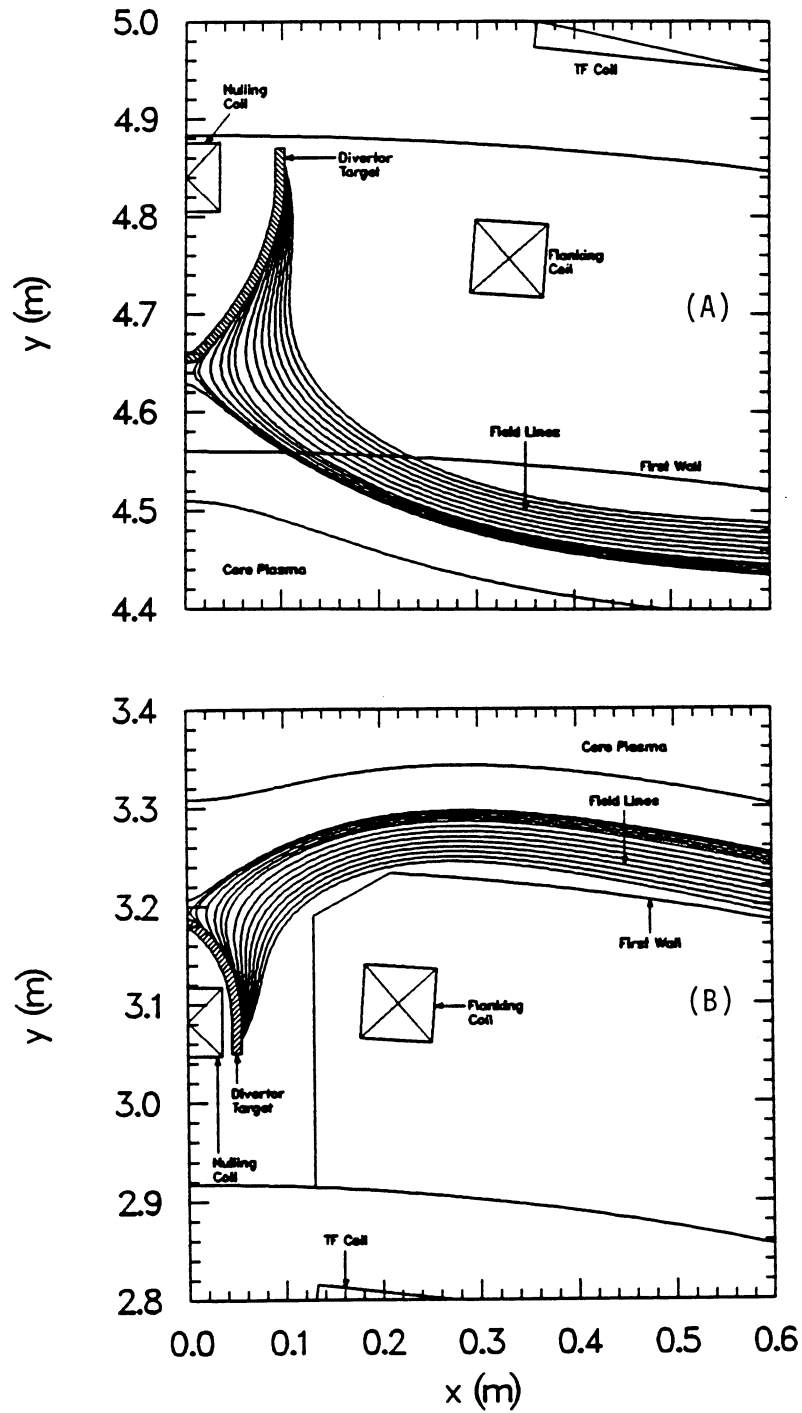


Figure 17.4-1. Outboard (A) and inboard (B) graph) equatorial-plane views of the divertor region for TITAN-II.

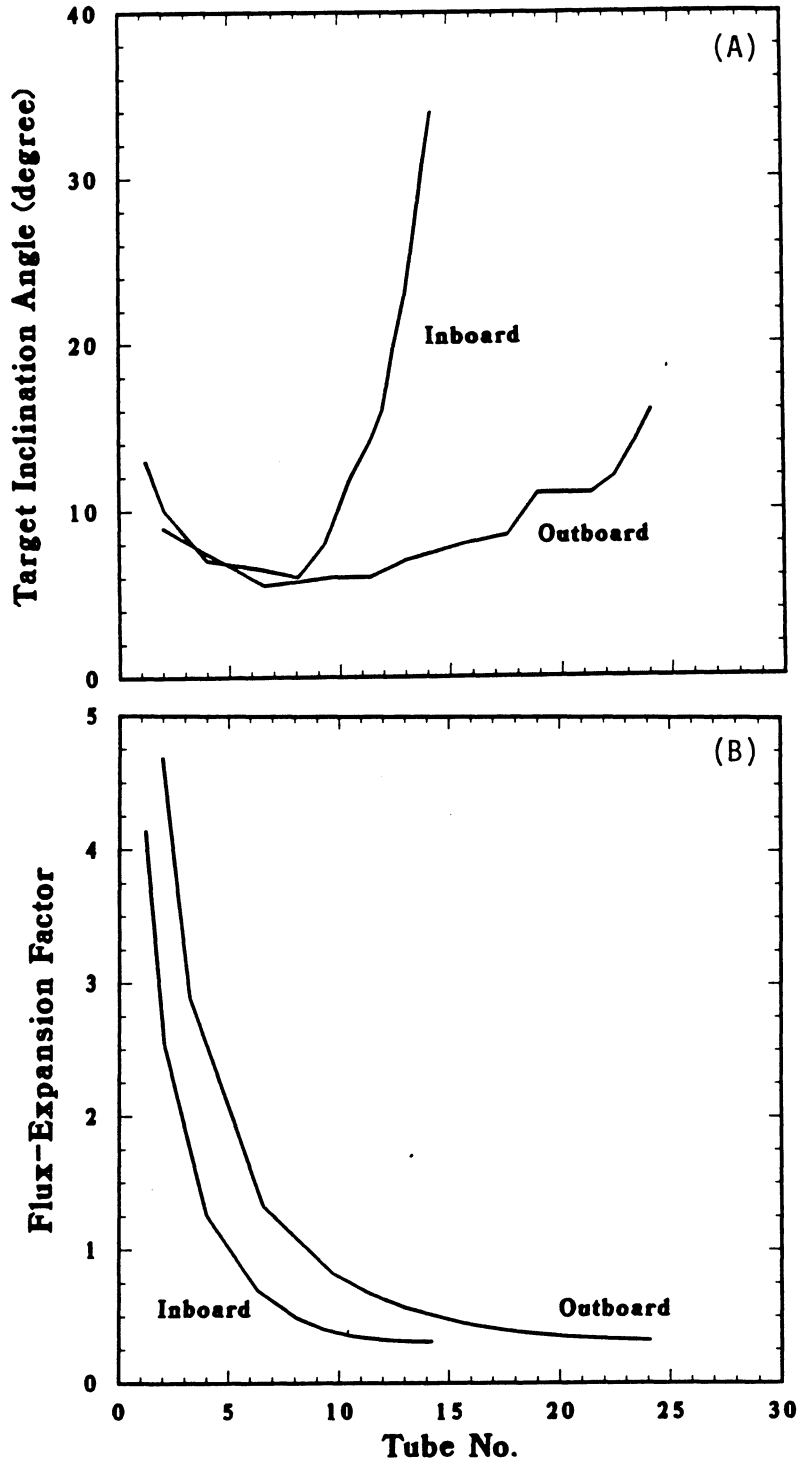


Figure 17.4-2. Target-inclination angle (A) and flux-expansion factor (B) as a function of position along inboard and outboard sections of TITAN-II divertor target. The distance is measured along the target from its apex.

of 10 mm and a wall thickness of 1 mm. Subsequent stress analysis (Section 17.5) indicated that with a 1-mm-thick W-26Re armor plate bonded to these tubes, the equivalent thermal stress on the inboard part of the target approached the design limit of 600 MPa. Therefore, total thickness of high-Z sputtering-resistant material is 2 mm, the same as for TITAN-I, although some of this layer performs a structural function. The detailed stress analysis, however, shows that the pressure stresses are well within the design limits, and a substantial fraction of the tube wall would have to be eroded before any failure occurred. As the erosion allowance was specified on the very conservative grounds of ignoring re-deposition, which may be expected to be extensive, the TITAN-II design appears to be acceptable.

To accommodate the high heat loads on the divertor target, advantage is taken of the high heat-transfer coefficients possible in the subcooled-flow-boiling regime, as used in the first-wall cooling. At any point along the coolant tube, the heat-transfer coefficient is taken as the greater of the values predicted by the Dittus-Boelter (forced-convection) correlation and the Thom correlation for subcooled flow boiling.

The Dittus-Boelter correlation is given by

$$Nu = 0.023 Re^{0.8} Pr^{0.4}, \quad (17.4-1)$$

where  $Nu$ ,  $Re$ , and  $Pr$  are, respectively, the Nusselt, Reynolds, and Prandtl numbers. The Thom correlation for the tube-wall superheat,  $T_w - T_{sat}$ , in subcooled flow boiling is [21]

$$T_w - T_{sat} = 22.65 \sqrt{q''} e^{-p/8.69}, \quad (17.4-2)$$

where  $q''$  is the heat flux into the coolant ( $MW/m^2$ ) and  $p$  is the coolant pressure (MPa). These correlations can be used to determine the temperature of the inner wall of the coolant tube (tube-coolant interface) and a 1-D thermal analysis, as described in Section 11.4, is then used to evaluate the temperature distribution through the tube wall and armor.

For any water-cooled component, it is important that the heat flux into the coolant is maintained below the critical heat flux (CHF) for the particular conditions. In the absence of any CHF correlations specifically for high-temperature aqueous solutions, a general correlation, derived for water, has been used to assess the cooling performance of the TITAN-II divertor target. This correlation for the CHF,  $q''_{CHF}$ , was developed by Jens and Lottes [22]. Conversion to more convenient units of  $MW/m^2$  yields

$$q''_{CHF} = C \left( \frac{G}{1356} \right)^m (\Delta T_{sub})^{0.22}, \quad (17.4-3)$$

where  $G$  is the mass velocity of the coolant ( $= \rho v$ ) in  $\text{kg}/\text{m}^2 \text{ s}$ , the factor 1356 arises from the conversion of units, and  $\Delta T_{sub}$  is the subcooling in  $^{\circ}\text{C}$ . Constants  $C$  and  $m$  depend on the pressure,  $p$ , through

$$C = 3.00 - 0.102 p, \quad (17.4-4)$$

$$m = \frac{p}{30} + 0.04. \quad (17.4-5)$$

To allow for uncertainties in the correlations and to include a safety margin in the design, the allowable heat flux is generally assumed to be lower than the estimated CHF limit by a factor  $\sim 1.4$  for water-cooled systems. For the TITAN-II design, the same factor has been used in the analysis, although the application of the water-derived CHF correlation to the salt-solution coolant increases the uncertainty.

A further factor in considering CHF's is the conduction of heat from the surface of the target into the coolant. In general, the heat flux tends to be concentrated from the value on the surface to a smaller area of the tube inner wall (Section 17.5). This peaking, which is augmented by the gap between the coolant tubes, is included in the analysis by using an approximate fit to the concentration factor found by the finite-element analysis (Section 17.5). Note that this concentration is only of importance for CHF considerations; for the lithium-cooled TITAN-I divertor, the only impact would be to increase the temperature drops across the structure by a small amount.

Figure 17.4-3 shows the distribution of heat flux along the divertor targets for the inboard and outboard locations shown in Figure 17.4-1. The distance along the target is measured in the direction of the coolant flow (*i.e.*, the center of the figure, where the heat flux drops, is at the apex of the target) facing directly into the core plasma. Figure 17.4-3 shows that the maximum total surface heat flux on the inboard target is  $7.5 \text{ MW}/\text{m}^2$  with  $5.8 \text{ MW}/\text{m}^2$  of the heat flux on the outboard target (compared with corresponding levels of  $9.5$  and  $6.0 \text{ MW}/\text{m}^2$  for TITAN-I). This reduction in the divertor-plate surface heat flux for TITAN-II was made possible by the increased freedom in shaping the target, allowing it to be located in areas of higher magnetic field than would have been permitted for the liquid-metal-cooled TITAN-I. Figure 17.4-3 also shows an estimate of the concentration in the heat flux (*i.e.*, the difference between the total surface heat flux and the inner-wall heat flux).

Given the heat loadings on the divertor-plate cooling tubes, the coolant conditions are determined by the requirements of obtaining an adequate safety factor on CHF, and of allowing the heat deposited into the divertor-target-coolant loop to be removed by a heat exchanger with the inlet coolant for the blanket. Additional constraints were

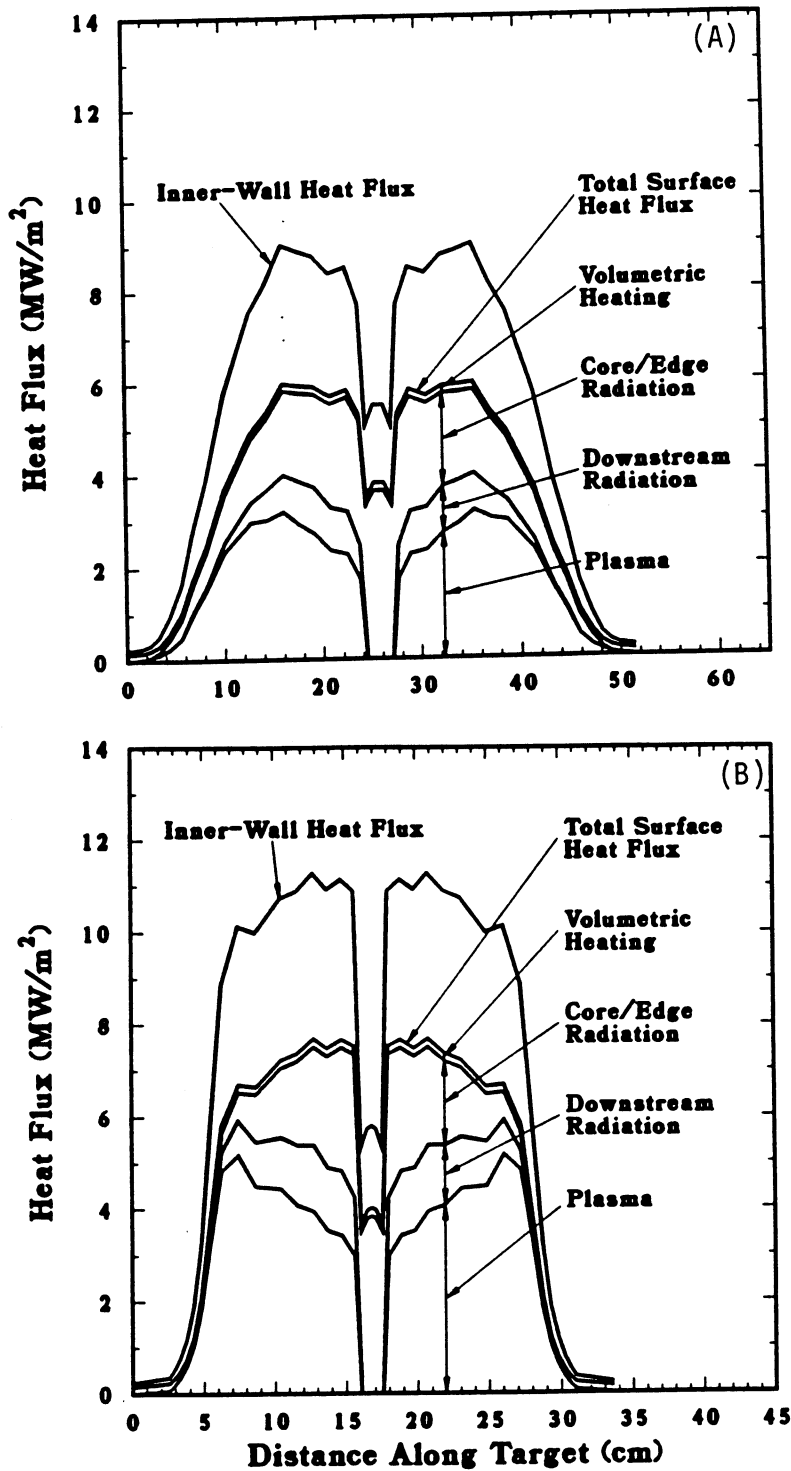


Figure 17.4-3. Heat flux distribution on outboard (A) and inboard (B) sections of divertor target. The CHF for TITAN-II divertor coolant is estimated at  $16.2 \text{ MW/m}^2$  (Equation 17.4-3). Distance along target is measured in the direction of coolant flow.

that the coolant velocity should not exceed 20 m/s and that its composition should be the same as for the blanket (6.4 at.% Li). These considerations led to the selection of the coolant-outlet conditions of 345 °C and 14 MPa. At this pressure, the boiling point of a 6.4% LiNO<sub>3</sub> solution is 405 °C (Section 16.2), yielding a subcooling at the outlet conditions of 60 °C and a CHF of 16.2 MW/m<sup>2</sup>, as predicted by the Jens and Lottes correlation (Equation 17.4-3). Figure 17.4-3 indicates that a safety factor in excess of 1.4 with respect to CHF is achieved at all points on the target; on the outboard target, where the heat fluxes are lower, the minimum safety factor is about 1.8.

Figure 17.4-4 shows the coolant and structure temperatures as a function of distance along the inboard and outboard divertor targets. The coolant-temperature rise along the tube is about 7 °C, while the saturation temperature remains virtually constant because the pressure drop along the tube is small. The heat removed from the divertor plate is deposited into the blanket-cooling circuit through a heat exchanger. In order to maintain a minimum temperature difference of 20 °C in the heat exchanger between the inlet divertor coolant and the inlet blanket coolant (298 °C), the divertor-coolant inlet temperature must be not less than 318 °C. For a divertor-coolant exit temperature of 345 °C and temperature rise of about 7 °C per pass, the TITAN-II divertor coolant passes four times across the target. The temperature of the inner wall of the coolant tube is governed by the local heat flux, and the abrupt change in slope in Figure 17.4-4 is caused by the onset of subcooled flow boiling, which prevents the wall temperature from rising to a level substantially above the saturation temperature.

The maximum temperature of the armor is estimated to be ~ 660 °C. This is somewhat lower than the result from the finite-element thermal analysis, described below in Section 17.5, because of 2-D effects in the heat conduction and because the gaps between the tubes have been ignored in this calculation.

## 17.5. THERMAL AND STRUCTURAL ANALYSES

The overall geometry of the TITAN-II divertor is very similar to that for TITAN-I, but there are two major differences: (1) the TITAN-II divertor is manufactured from a single material; (2) the coolant flow is in the radial/toroidal direction, rather than poloidal, thus destroying the axisymmetry of the TITAN-I design (Section 11.5) and requiring a somewhat different finite-element modeling. The finite-element analysis was performed for the inboard section of the divertor target where the heat loadings are the highest.

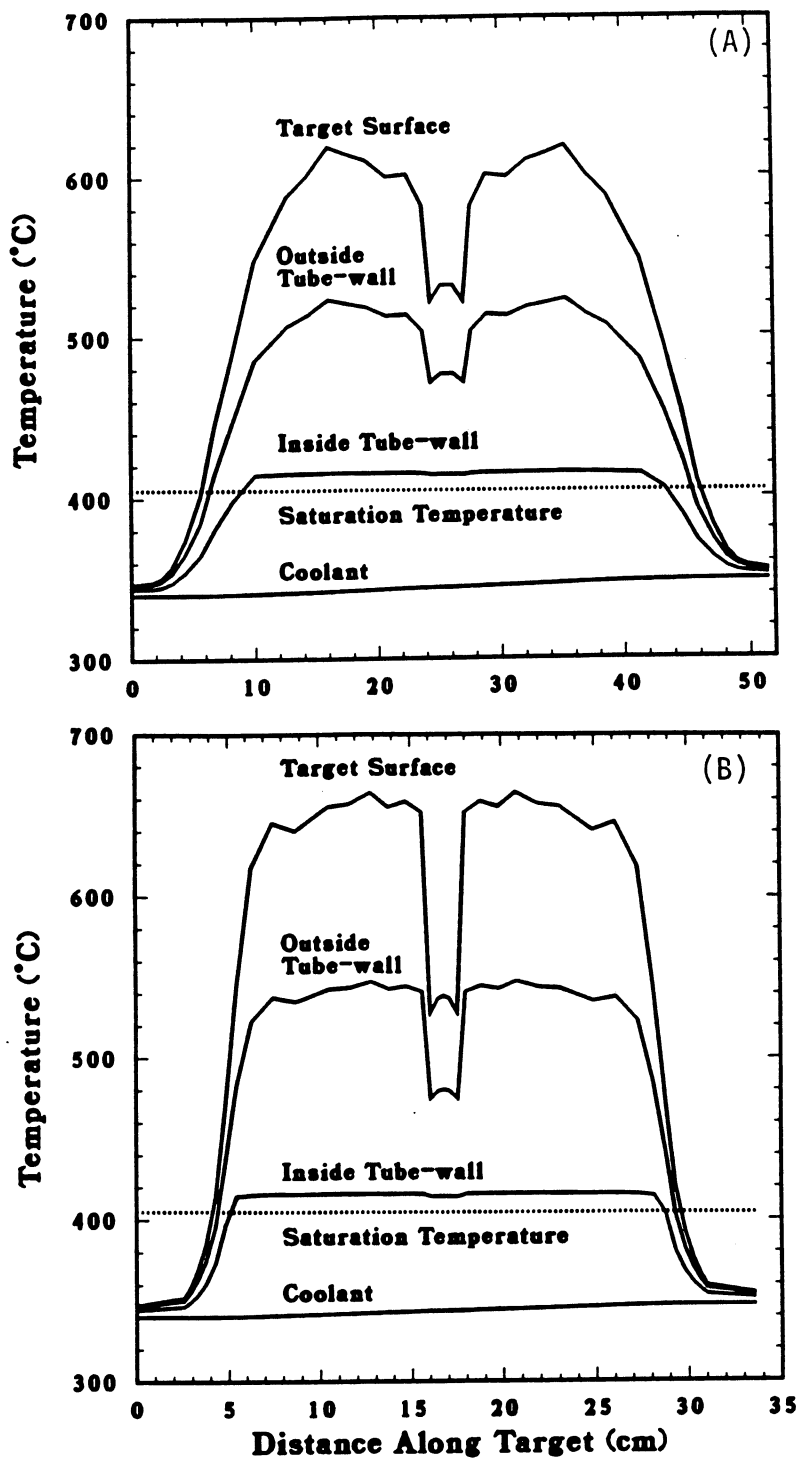


Figure 17.4-4. Coolant and structure temperature distribution on outboard (A) and inboard (B) sections of the divertor target. Distance along target is measured in the direction of coolant flow.

### 17.5.1. Thermal Analysis

The surface heat flux on the inboard section of the TITAN-II divertor target (distance measured from the apex in the toroidal direction) is shown in Figure 17.4-3. The surface heat flux shows a broad peak of 7.5 MW/m<sup>2</sup>, covering about 8 cm of the inboard target. Because the thickness of the divertor plates (0.2 cm) is much smaller than the distance over which this heat flux changes appreciably, a detailed model such as that used for TITAN-I should be quite accurate (Section 11.5).

The finite-element model used for the thermal analysis is shown in Figure 17.5-1. The heat flux is assumed to be uniform over the plasma-facing surface and the lines of symmetry on the sides are assumed to be adiabatic. The heat-transfer coefficient at the interface between the tube wall and the coolant was set to be the greater of the two coefficients calculated from subcooled-flow-boiling and laminar-flow correlations. In other words, boiling is assumed to occur in regions of the tube where the subcooled-flow-boiling correlation predicts a higher heat-transfer coefficient than the forced-convection correlation. For the TITAN-II divertor, the Dittus-Boelter correlation (Equation 17.4-1) predicts a heat-transfer coefficient of 57 kW/m<sup>2</sup>-K. For subcooled flow boiling, the heat-transfer coefficient was calculated from Thom's correlation [23] which, for 60 °C of subcooling and 14 MPa of coolant pressure, is

$$h = \frac{q}{60 + 4.54 \sqrt{q}}, \quad (17.5-1)$$

where  $q$  is the local heat flux (MW/m<sup>2</sup>) and  $h$  is the heat-transfer coefficient (MW/m<sup>2</sup> K). This value for the heat-transfer coefficient has been normalized by the ratio of the subcooling to the film temperature drop, so it can be used in a finite-element code which assumes that the heat-transfer correlations are based on the film temperature drop.

Because the boiling heat-transfer correlation is based on the local heat flux which is not known, an iterative solution method is required. The local heat flux into the coolant along the inside wall of the coolant tube is first estimated, assuming it peaks at the apex of the tube (the point nearest to the plasma) and drops to zero at an angle of about 60° to either side of the peak. From this estimated local heat-flux distribution, the heat-transfer coefficient is calculated around the tube and input to the finite-element code. The resultant heat fluxes from the finite-element analysis are then used to update the heat-transfer coefficients and the problem is recalculated. This process is repeated until the desired accuracy is achieved. In practice, the local heat fluxes seemed to depend only on the geometry, rather than on the heat-transfer coefficient, so the local flux changed little after the initial run and convergence of this iterative process was rapid.

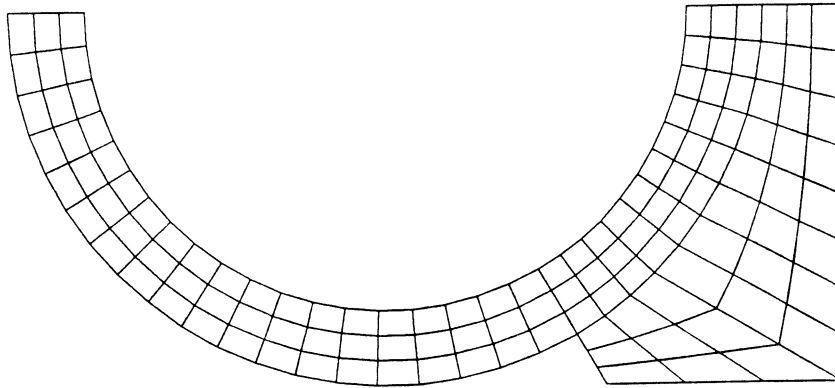


**Figure 17.5-1.** The finite-element model used for thermal and structural analyses of the TITAN-II divertor plate.

The temperature contours, for the coolant tubes touching each other, are shown in Figure 17.5-2. The peak temperature is  $762^{\circ}\text{C}$ , located at the divertor-plate surface midway between two neighboring tubes. A crucial aspect of the thermal analysis for the TITAN-II divertor is that the maximum local heat flux into the coolant must be well below the CHF limit of  $\sim 16 \text{ MW}/\text{m}^2$ . The maximum local heat flux is greater than the surface heat flux of  $7.5 \text{ MW}/\text{m}^2$  for two reasons:

1. The area available for transfer of heat into the coolant is less than the area facing the plasma. Assuming that only about  $65^{\circ}$  of the inner wall on either side of the apex actually conducts heat into the coolant (as indicated by the finite-element calculations), this effect would amplify the peak heat flux to over  $8 \text{ MW}/\text{m}^2$ .
2. The heat tends to flow into the coolant along radial paths, rather than flowing perpendicular to the plasma-facing surface, thus resulting in the concentration of the heat flux towards the apex of the tube.

The distribution of the heat flux into the coolant (or at the inner wall of the coolant tube) is shown in Figure 17.5-3. One of the curves in this figure corresponds to the case of the heat flux on the top surface entering the tube with a pure cosine distribution, as would be expected for a thin-walled tube. This curve shows a peak heat flux of over  $9 \text{ MW}/\text{m}^2$ , which is well above the surface heat flux of  $7.5 \text{ MW}/\text{m}^2$ . This increase in the heat flux is a result of the decrease in the surface area caused by the difference between the outer and inner radii of the tube. For the TITAN-II divertor plate, the finite-element

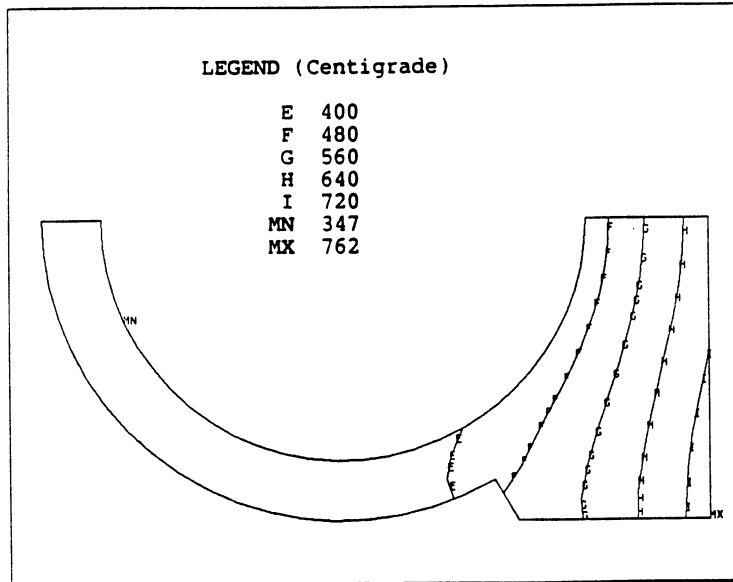


Figure 17.5-2. Temperature contours for the TITAN-II divertor plate from the finite-element analysis for a surface heat flux of  $7.5 \text{ MW/m}^2$  and no gap between neighboring tubes.

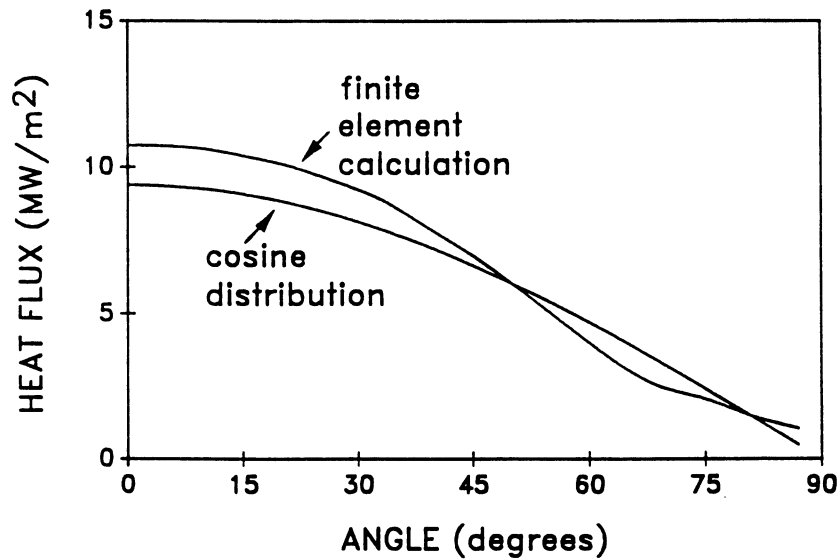


Figure 17.5-3. Distribution of the heat flux into the coolant along the inner surface of the coolant tube of the TITAN-II divertor from the finite-element analysis for a surface heat flux of  $7.5 \text{ MW/m}^2$  and no gap between neighboring tubes.

calculations show that the enhancement in the heat flux at the point closest to the plasma is even more pronounced because the tube wall is effectively very thick at the plasma-facing surface (second curve in Figure 17.5-3). For this case, the peak heat flux into the coolant is  $10.7 \text{ MW/m}^2$ , thus providing a safety margin of about 1.5 with respect to the CHF ( $16.2 \text{ MW/m}^2$ ).

Because of the double curvature of the divertor target, there would be a gap between the constant-cross-section coolant tubes everywhere except at the apex (the points of minimum minor radius). At the points of the maximum heat flux, located 2 to 6 cm away from the apex in the radial/toroidal direction (Figure 17.4-3), there is a small gap (0.4 mm) between neighboring tubes, as can be seen in Figure 17.3-1. The presence of this gap increases the maximum heat flux into the coolant to  $10.9 \text{ MW/m}^2$  and the peak structural temperature to  $779^\circ\text{C}$ , again providing a safety margin of about 1.5 with respect to the CHF ( $16.2 \text{ MW/m}^2$ ).

### 17.5.2. Stress Analysis

As with the thermal analysis, the boundary conditions and global deformations have little effect on the pressure stresses in the divertor. Hence, the detailed finite-element model used previously can also be used to calculate the primary stresses induced by the 14-MPa coolant pressure. The equivalent stress contours are shown in Figure 17.5-4. The peak stress is 83 MPa. There is some bending in the tube wall, thus increasing the peak primary stress above the expected value of 56 MPa (from  $\sigma = pr/t$ ). Also, the primary stress in the plasma-facing surface, which will be shown to be the location of the peak thermal stress, is essentially zero.

Because the coolant flow in the TITAN-II divertor plate is in the radial/toroidal direction, there is no poloidal axisymmetry in the structure, and the detailed model used for the thermal analysis cannot be used for calculating the thermal stresses which depend strongly on the imposed boundary conditions. Fortunately, the coolant tubes, themselves, have little effect on the thermal stress distribution (as indicated by preliminary analyses) so an axisymmetric model can be used to approximate the structural behavior of the divertor plate as a unit. This allows accurate treatment of the boundary constraints without a prohibitive loss of detail.

The finite-element model which is used to analyze the thermal stresses is shown in Figure 17.5-5. Half of the U-shaped cross section is modeled by using symmetry conditions to model the other half. The model consists of 600 axisymmetric quadrilateral

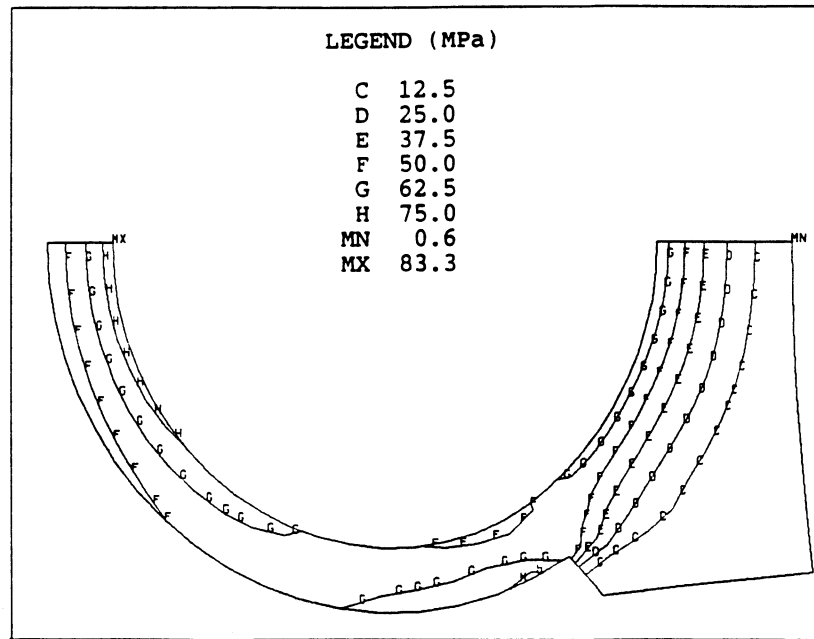


Figure 17.5-4. Equivalent pressure-stress contours from finite-element analysis of the TITAN-II divertor plate for a coolant pressure of 14 MPa.

elements. The heat flux was distributed along the surface of the divertor according to Figure 17.4-3 (also shown in Figure 17.5-6) and a constant heat-transfer coefficient of  $200 \text{ kW/m}^2$  was assumed along the entire inner surface. The bulk temperature of the coolant was assumed to be  $345^\circ\text{C}$ .

The maximum temperature is  $615^\circ\text{C}$  and occurs at point A on Figure 17.5-5. The temperature drops across the divertor-plate structural material is  $229^\circ\text{C}$ , which is  $36^\circ\text{C}$  lower than the calculated value from the local analysis ( $265^\circ\text{C}$ ). Hence, the global model will underestimate the in-plane stresses by roughly the same amount (15%). The out-of-plane stresses, though, tend to dominate the equivalent stresses in this problem, and they would be underestimated by less than 15% because these stresses depend on the overall temperature distribution, rather than just the local distribution.

The peak equivalent stresses in the TITAN-II divertor plate occur on the plate surface and are shown in Figure 17.5-6. The maximum equivalent stress, which occurs at the same location as the peak temperature, is 505 MPa. Since the pressure stress at this point is zero, the allowable stress at this location is  $3S_{mt} = 600 \text{ MPa}$  for tungsten. Therefore, the TITAN-II divertor plate can withstand the very high heat fluxes expected during the normal operation.

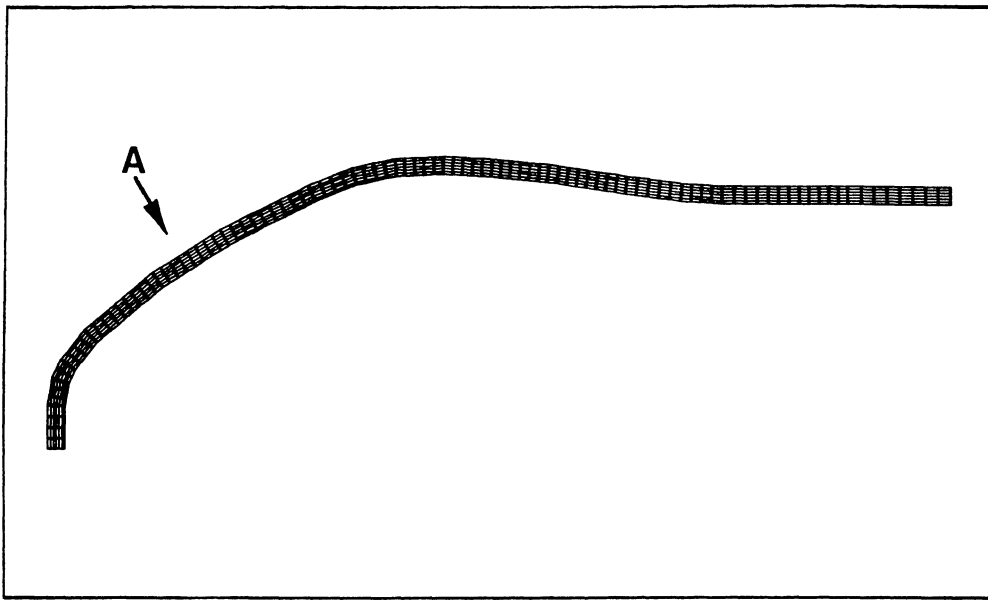


Figure 17.5-5. Finite-element model for determination of thermal stresses in the TITAN-II divertor plate.

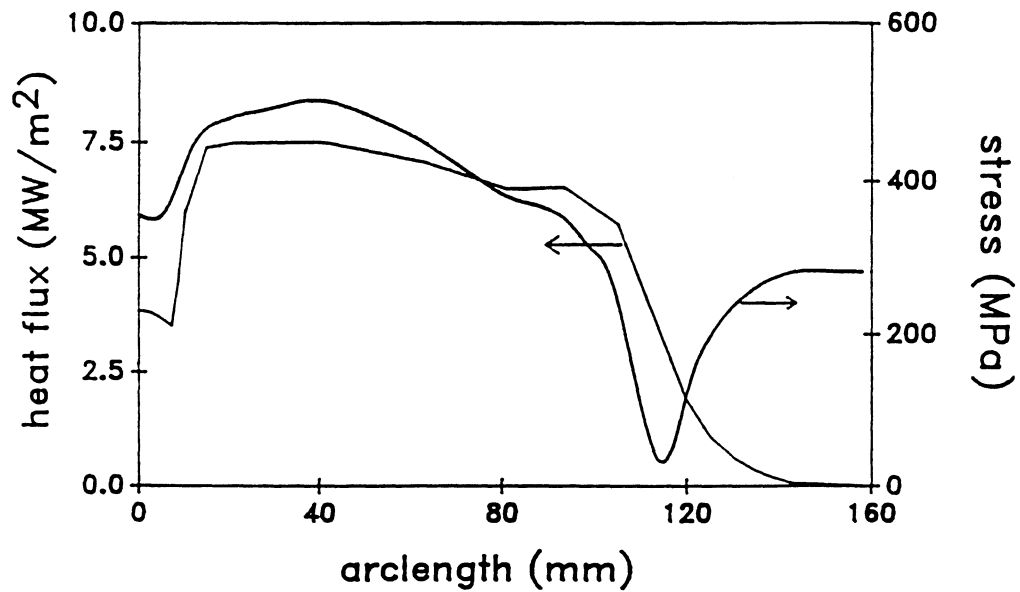


Figure 17.5-6. Surface heat flux and peak-equivalent thermal-stress distributions on the inboard section of the TITAN-II divertor. Distance along the target is measured in the radial/toroidal direction from the apex.

## 17.6. DIVERTOR-COIL ENGINEERING

The toroidal-field-coil design for TITAN-II, which consists of copper coils as opposed to the IBCs of TITAN-I, prompted a new divertor magnetic design (reported fully in Section 4.4). The final magnetic design, similar to that of TITAN-I, includes three divertor modules, located  $120^\circ$  apart in the toroidal direction. An equatorial-plane cross section of the divertor coils is shown in Figure 17.1-1. The magnetic field lines are diverted onto the divertor plate using one nulling and two flanking coils which localize the nulling effect. No divertor-trim coils are needed for the TITAN-II design. The use of copper divertor coils reduces the joule losses in the TITAN-II divertor coils to 9.8 MW which are much smaller than that of the TITAN-I design (120 MW).

The TITAN-II divertor coils are normal-conducting copper coils cooled by pure water with spinel insulator material. Because of the expected long life of the inorganic spinel insulator (Section 10.2.3), the TITAN-II divertor coils are expected to perform at the design level for the one-year lifetime of the divertor module. The nuclear heating in the divertor coils is not excessive and can easily be removed by the cooling circuit.

Forces on the divertor coils are of four types: (1) outward radial forces on each coil caused by the interaction of the coil current with the toroidal field, (2) centering forces resulting from the radial variation of the toroidal field, (3) overturning moments generated by the interaction between the vertical field and the coil current, and (4) out-of-plane forces caused by the spatial variation of the magnetic field especially in the divertor region. These electromagnetic forces also vary in time during the cycles of the oscillating-field current-drive (OFCD) system.

The forces exerted on the divertor coils are such that the maximum coil face pressure is of the order of 1.8 MPa. This constitutes only about 3% of the end forces generated by the blanket-coolant pressure (Section 16.4). Capturing the flanking coil against the end wall within the blanket scarcely alters the loading patterns in the blanket and the blanket-load paths can be easily strengthened to accommodate this small increase. Figure 17.6-1 shows the equatorial-plane view of the TITAN-II divertor module and the related structure. The structural support for the nulling coil is also explicitly shown. The nulling coil does not see any lateral forces.

The spine plate and shield block behind the nulling coil serve to maintain the shape of this coil and resist its tendency to translate outwards. This spine plate and shield block cover the entire divertor circumference but are restricted to the divertor-plate width on the outboard section to allow for the divertor pumping ducts. As illustrated in

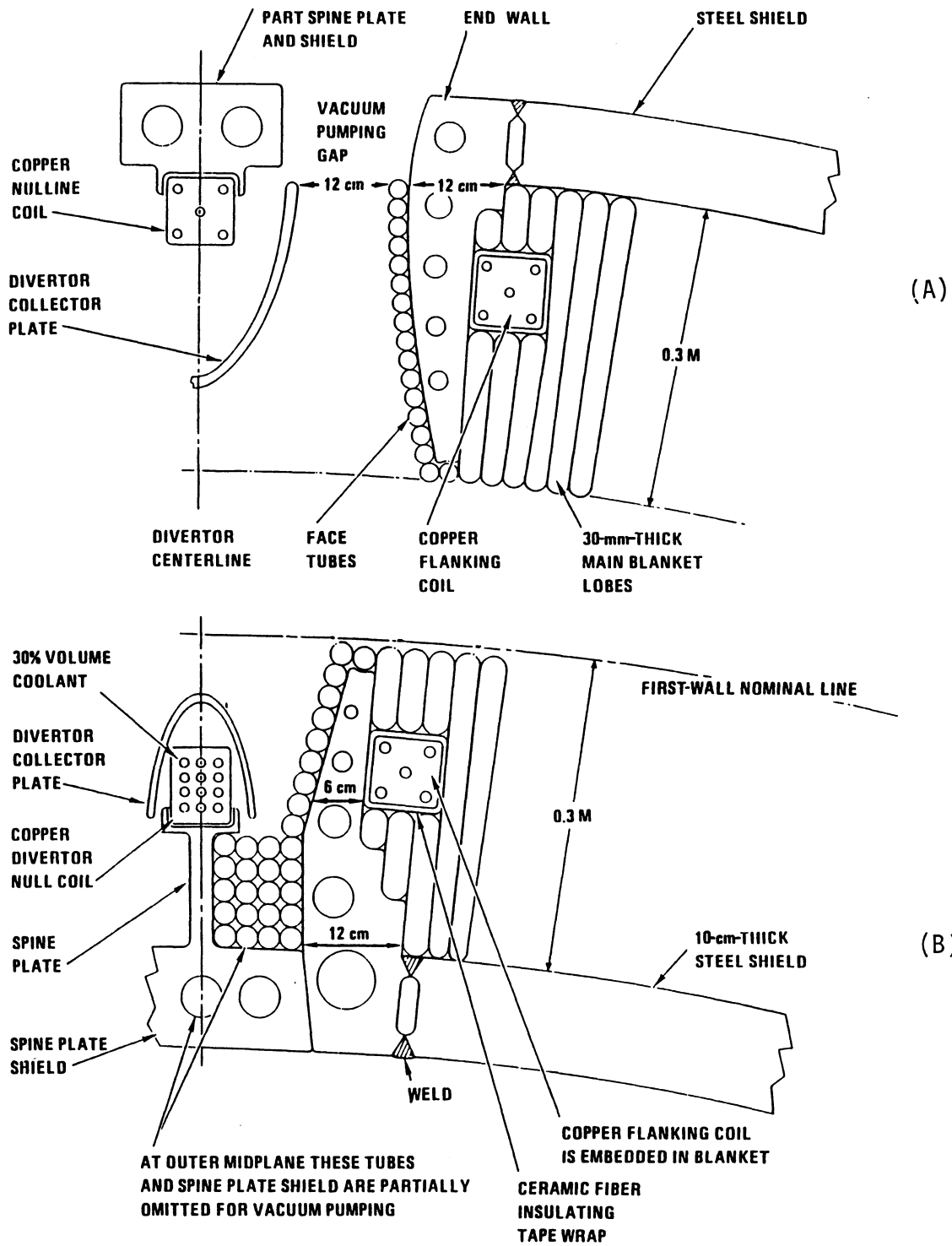


Figure 17.6-1. Equatorial-plane views of outboard (A) and inboard (B) cross sections of the divertor modules and the related support structure.

Figure 17.6-1, some face tubes are needed in the divertor module in order to handle the surface heat flux and also to fill in voids around the back of the divertor collector plates.

## 17.7. VACUUM SYSTEMS

The vacuum boundary in the TITAN-II design is behind the hot shield, as opposed to the TITAN-I design in which the entire fusion power core (FPC) is located inside a vacuum tank. Three vacuum-pumping ducts with large cross sections are connected to the outboard side of the three divertor modules of TITAN-II. The high-vacuum pumps are connected to these ducts and are located under the water pool surrounding the TITAN-II FPC to allow easy access for maintenance. This arrangement also minimizes the shielding requirements because the water pool surrounding the TITAN-II FPC also acts as a very good radiation shield. Detailed calculations for the pumping requirements of the TITAN-II design have not been performed but they are not expected to be very different from those of the TITAN-I design.

## 17.8. SUMMARY AND CONCLUSIONS

The design of the impurity-control system poses some of the most severe problems of any component of a DT fusion reactor. For TITAN-II design, the impurity-control system is based on toroidal-field divertors in order to minimize the perturbation to the global magnetic configuration, and to minimize the coil currents and stresses. Three such divertors are used as a compromise between the conflicting desires to minimize the joule losses in the divertor coils and maximize the total area of divertor plates.

To limit the heat flux on the divertor-target plate to a manageable level ( $10 \text{ MW/m}^2$ ), the TITAN plasma is required to operate in a high-radiation regime, such that a total of about 95% of the steady-state heating power is radiated in the core, edge, and divertor plasmas. An "open" configuration, in which the divertor target is located close to the null point in the magnetic field, is used, rather than a "closed" configuration, which tends to produce large peaking factors in the heat-flux distribution. These features, together with careful shaping of the divertor-target surface, allow the maximum heat flux at the inboard location to be limited to  $7.5 \text{ MW/m}^2$ , with a peak outboard value of  $5.8 \text{ MW/m}^2$ .

To satisfy the requirement for a high-Z material for the plasma-facing surface of the divertor target, a tungsten-rhenium alloy, W-26Re, is used. The high rhenium content

provides the high ductility and high strength necessary for the severe loading conditions. A single structural material is used for the divertor target to avoid the problems of bonding dissimilar materials and of stress concentrations which occur at the interface of the two materials. The coolant tubes are, therefore, also made from W-26Re alloy.

The coolant for the divertor system is an aqueous-LiNO<sub>3</sub> solution, as used in the TITAN-II blanket. Advantage is taken of the predicted differences in the physical properties between this solution and pure water to obtain the high CHF's ( $\sim 16 \text{ MW/m}^2$ ) necessary to provide an adequate safety margin against burnout. The divertor-plate coolant flows in the toroidal/radial direction to equalize the power deposited on each tube, although this causes gaps between adjacent tubes (if they are of constant cross section) because of the double curvature of the divertor plate. Fabrication of the divertor target is based on brazing of the tungsten-alloy plate (which is produced by powder-metallurgy techniques) to a bank of constant-cross-section coolant tubes, although alternative methods which allow tubes of variable cross section to be constructed have also been considered.

Two-dimensional, finite-element thermal and structural analyses were performed, which indicated that the maximum equivalent thermal stress is about 500 MPa, within the allowable level of 600 MPa for tungsten. The thermal analysis showed that geometric effects concentrate the heat flux from its value on the plate surface to a higher value at the tube-coolant interface, and that the effects of the gaps between adjacent tubes in elevating structural temperatures are acceptable.

In conclusion, at the present level of analysis, the toroidal-field divertor design for TITAN-II appears to represent a feasible design approach for the impurity-control and particle-exhaust system for a high-power-density reversed-field-pinch (RFP) reactor. A number of areas require further analysis and experimental investigation to confirm their potential as described in this report. Demonstration of good RFP operation with a toroidal-field divertor is clearly necessary, and operation with a highly radiative core plasma is central to the divertor design and also requires further experimental work.

The physical and heat-transfer properties of LiNO<sub>3</sub> solutions need to be better understood, although the present estimates suggest they should be favorable. The fabrication procedure proposed for manufacturing the large divertor plate from tungsten-rhenium alloy requires experimental verification, and the data base for the irradiated properties of the tungsten alloy requires considerable expansion. Additional work on the design of the support structure for the divertor modules and the divertor coils and the vacuum system is also needed.

**REFERENCES**

- [1] "Tungsten-Rhenium Alloys," in *Refractory Metals and Special Metals*, Metallwerk Plansee GmbH, Austria (1987).
- [2] "How to Make Time with Tungsten," in *A Practical Guide on the Various Uses of Tungsten*, Schwarzkopf Development Corporation, Holliston, MA (1987).
- [3] G. Orient, Rockwell International, private communications (1987).
- [4] W. Kern and V. S. Ban, "Chemical Vapor Deposition of Inorganic Thin Films," *Thin Film Processes*, Academic Press, New York (1978) p. 257.
- [5] "Chemical Vapor Deposition of Refractory Metals, Alloys and Compounds," in *Proc. Am. Nucl. Soc.*, A. W. Shaffhauser (Ed.), Hinsdale, IL (1967).
- [6] "Chemical Vapor Deposition - Second International Conference," in *Proc. Conf. Electrochem. Soc.*, J. M. Blocher, Jr. and J. C. Withers (Eds.), New York, NY (1970).
- [7] "Chemical Vapor Deposition - Third International Conference," in *Proc. Conf. Electrochem. Soc.*, F. A. Glaski (Ed.), Hinsdale, IL (1972).
- [8] "Chemical Vapor Deposition - Fourth International Conference," in *Proc. Conf. Electrochem. Soc.*, G. F. Wakefield and J. M. Blocher Jr. (Eds.), Princeton, NJ (1973).
- [9] "Chemical Vapor Deposition - Fifth International Conference," in *Proc. Conf. Electrochem. Soc.*, J. M. Blocher, Jr., H. E. Hintermann, and L. H. Hall (Eds.), Princeton, NJ (1975).
- [10] R. C. Svedberg and R. W. Buckman Jr., "W-Re Composite Tube Fabrication by Chemical Vapor Deposition for Application in an 1800°C High Thermal Efficiency Fuel-Processing Furnace," *Thin Solid Films* **72** (1980) 393.
- [11] J. I. Federer and A. C. Schaffhauser, "Chemical Vapor Deposition and Characterization of Tungsten-Rhenium Alloys," *Proc. Int. Conf. on CVD*, Salt Lake City, UT (April 1977) 242.
- [12] F. A. Glaski, "A Report on the Current Role of Chemical Vapor Deposition as a Manufacturing Process," *Proc. Conf. CVD of Refractory Metals, Alloys and Compounds*, Gatlinburg, TN (September 1967) 276.

- [13] H. E. McCoy and J. O. Stiegler, "Mechanical Behavior of CVD Tungsten at Elevated Temperatures," *Proc. Conf. CVD of Refractory Metals, Alloys and Compounds*, Gatlinburg, TN (September 1967) 391.
- [14] A. C. Schaffhauser, "Low-Temperature Ductility and Strength of Thermochemically Deposited Tungsten and Effects of Heat Treatment," *Summary of 11th Refractory Composites Working Group Meeting*, AFML-TR-66-179 (July 1966) 261.
- [15] W. R. Holman and F. J. Huegel, "CVD Tungsten and Tungsten-Rhenium Alloys for Structural Applications. Part I: Process Development," *Proc. CVD of Refractory Metals, Alloys and Compounds*, Gatlinburg, TN (September 1967) 127.
- [16] W. R. Holman and F. J. Huegel, "CVD Tungsten and Tungsten-Rhenium Alloys for Structural Applications. Part II: Evaluation," *Proc. CVD of Refractory Metals, Alloys and Compounds*, Gatlinburg, TN (September 1967) 427.
- [17] F. J. Huegel and W. R. Holman, "CVD Tungsten and Tungsten-Rhenium Alloys for Structural Applications. Part III: Recent Developments," *Proc. CVD of Refractory Metals, Alloys and Compounds*, Gatlinburg, TN (September 1967) 171.
- [18] F. A. Glaski, "A Report on the Current Role of Chemical Vapor Deposition as a Manufacturing Process," *Proc. CVD of Refractory Metals, Alloys and Compounds*, Gatlinburg, TN (September 1967) 276.
- [19] A. M. Shroff, "Vapor Deposition of Refractory Materials," *Proc. 6th Plansee Seminar* (1968) 845.
- [20] L. W. Roberts, "The Properties of CVD Deposits of W and W-Re alloys," *Proc. 6th Plansee Seminar* (1968) 880.
- [21] J. G. Collier, *Convective Boiling and Condensation*, McGraw-Hill, London (1972) p. 159.
- [22] W. H. Jens and P. A. Lottes, "Analysis of Heat Transfer, Burnout, Pressure Drop and Density Data for High Pressure Water," U. S. Atomic Energy Commission report ANL-4627 (1951).
- [23] J. R. S. Thom, W. M. Walker, T. A. Fallon, and G. F. S. Reising, "Boiling in Subcooled Water During Flow in Tubes and Annuli," *Proc. Inst. Mech. Engr.* **3C** **180** (1965-66) 226.